Chinese Journal of
POLYMER SCIENCE

RESEARCH ARTICLE

https://doi.org/10.1007/s10118-025-3522-4
Chinese J. Polym. Sci. **2026**, *44*, 407–415

Water-soluble Polymer Ligand Mediated Synthesis of Superparamagnetic Iron Oxide Nanoparticles for Magnetic Resonance Imaging

Ping-Ting Gong[a,b,†], Jiao-Jiao Guo[a,†], Chang Gao[a,b,c], Wei-Tao Yang[d*], Chun-Sheng Xiao[e*], Yi Xu[f], Yue Yao[f], Irshad Hussain[g], Wen Fan[a], and Wei Yan[a,b,c*]

[a] *Key Laboratory of Green Preparation and Application for Functional Materials of Ministry of Education, Hubei Key Laboratory of Polymer Materials, School of Material Science and Engineering, Hubei University, Wuhan 430062, China*
[b] *Shenzhen Huazhong University of Science and Technology Research Institute, Shenzhen 518038, China*
[c] *Manchester Metropolitan Joint Institute, Hubei University, Wuhan 430062, China*
[d] *Department of Radiology, Tongji Hospital, Shanghai Frontiers Science Center of Nanocatalytic Medicine, the Institute for Biomedical Engineering & Nano Science, School of Medicine, Tongji University, Shanghai 200065, China*
[e] *State Key Laboratory of Polymer Science and Technology, Key Laboratory of Polymer Ecomaterials, Changchun Institute of Applied Chemistry, Chinese Academy of Sciences, Changchun 130022, China*
[f] *Department of Pathology, Li Ka Shing Faculty of Medicine, The University of Hong Kong, Hong Kong 999077, China*
[g] *Department of Chemistry and Chemical Engineering, SBA School of Science and Engineering, Lahore University of Management Sciences (LUMS). DHA, Lahore 54792, Pakistan*

Electronic Supplementary Information

Abstract Magnetic resonance imaging (MRI) is one of the most widely used diagnostic techniques. Iron oxide nanoparticles, as a promising kind of contrast agents, have attracted intense research interest due to their low toxicity and superparamagnetism. However, it is still a great challenge to prepare ideal iron oxide based contrast agents with high uniformity, excellent water solubility and biocompatibility. In this paper, a novel water-soluble polymer ligand pentaerythritol tetrakis 3-mercaptopropionate-poly(*N*-vinyl-2-pyrrolidone) (PTMP-PVP) was used as a capping reagent to prepare iron oxide nanoparticles MIONs@PTMP-PVP through one-step co-precipitation of iron precursors in aqueous solution at 100 °C. The obtained nanoparticles MIONs@PTMP-PVP had a small size and narrow size distribution, and they were found to be biocompatible as determined through CCK-8 assay and histology analysis. *In vivo* MRI study demonstrated that the obtained MIONs@PTMP-PVP can be potentially used as an effective T_2-weighted MRI contrast agent.

Keywords Iron oxide nanoparticles; Water-soluble polymer ligand; Magnetic resonance imaging

Citation: Gong, P. T.; Guo, J. J.; Gao, C.; Yang, W. T.; Xiao, C. S.; Xu, Y.; Yao, Y.; Hussain, I.; Fan, W.; Yan, W. Water-soluble polymer ligand mediated synthesis of superparamagnetic iron oxide nanoparticles for magnetic resonance imaging. *Chinese J. Polym. Sci.* **2026**, *44*, 407–415.

INTRODUCTION

Magnetic resonance imaging (MRI) is one of the most widely used diagnostic techniques in medical applications.[1–13] MRI contrast agents are a series of contrast media that can greatly improve the resolution and specificity of MRI by improving the relaxation rate of protons in the local tissues of the body.[14–18] There are many kinds of contrast agents, such as gadolinium(Gd)-based contrast agents and manganese contrast agents.[19–22] However, tissue toxicity and neurotoxicity limit their clinical applications. In terms of low toxicity,[23–26] super paramagnetic iron oxide nanoparticles (MIONs) have proved to be one of the most promising contrast agents and have been used clinically.[27–33] Iron oxide nanoparticles synthesized *via* the pyrolysis of organometallic iron precursors possess high uniformity and excellent magnetic properties, but the poor water solubility hampers their further biomedical applications.[34–37] Therefore, it is a great challenge to prepare ideal iron- oxide-based contrast agents with high uniformity, excellent water solubility, and biocompatibility.

In this study, we synthesized iron oxide particles by using co-precipitation method which is directly dispersed in the aqueous phase and is feasible for bio-applications.[38] The conventional co-precipitation method has some limitations, such as low monodispersity and low crystallinity due to the low reaction temperature and less control over the size of the particles. Fortunately, different types of protective molecules or capping ligands can be used to resolve these problems. There are several water-soluble and thioether-functionalized polymer ligands for the synthesis of MIONs with promising performance in MRI performance. Tan *et al*. prepared highly

* Corresponding authors, E-mail: weitaoyang@tongji.edu.cn (W.T.Y.)
E-mail: xiaocs@ciac.ac.cn (C.S.X.)
E-mail: willieyan2003@hubu.edu.cn (W.Y.)
† These authors contributed equally to this work.
Received October 25, 2025; Accepted November 30, 2025; Published online January 23, 2026

water-soluble magnetic iron oxide nanoparticles protected by dodecanethiol–polymethacrylic acid (DDT-PMAA), which were optimized to produce ultrasmall ((4.6±0.7) nm) MIONs with high magnetization (50 em·g^{-1}).[39] The obtained results indicated that these multifunctional MIONs with rich surface chemistry exhibit admirable potential in biomedical applications, including using as MRI contrast agents. They also reported the preparation of MIONs coated with a water-soluble thioether end-functionalized polymer ligand pentaerythritol tetrakis 3-mercaptopropionate-poly(methacrylic acid) (PTMP-PMAA).[40] The saturation magnetization of nanoparticles with TEM diameter 4.6 nm was found to be 45 em·g^{-1}. Li *et al*. also synthesized ultrasmall water-soluble and biocompatible MIONs modified with PTMP-PMAA as positive and negative dual contrast agents with very small size ((3.3±0.5) nm) and highlighted their potential as dual T_1–T_2 or T_1 contrast agents.[41] Although these systems enable the formation of MIONs with favorable dispersibility, they typically yielded nanoparticles with relatively small core sizes and limited magnetization, which restricts their effectiveness as T_2-weighted contrast agents, particularly for organ-specific imaging. Moreover, the lack of organ-targeting capability further limits their practical applicability. Therefore, it is essential to develop more suitable polymer ligands for regulating the nanoparticle size within a more appropriate size range, thereby enhancing both their magnetic properties and organ-specific imaging performance.

Among a series of polymer ligand, poly(*N*-vinyl-2-pyrrolidone) (PVP) is an important water-soluble polymer ligand that has been widely used as stabilizer for synthesis of magnetic iron oxide nanoparticles.[42–45] PVP has 2-pyrrolidone unit in its polymer chain backbone, which can effectively coordinate with iron oxide nanoparticles due to its high polarity. In this study, we used a novel trithiol and thioether end-functionalized water-soluble polymer, pentaerythritol tetrakis 3-mercaptopropionate-poly(*N*-vinyl-2-pyrrolidone) (PTMP-PVP), as a capping ligand for the preparation of iron oxide nanoparticles MIONs@PTMP-PVP through one-step co-precipitation of iron precursors in an aqueous solution at 100 °C (Scheme 1a). The obtained iron oxide nanoparticles had a small size and narrow size distribution, as observed by DLS and TEM, and they were found to be biocompatible, as determined through CCK-8 assay and histology analysis. *In vivo* MRI study (Scheme 1b) demonstrated that the obtained MIONs@PTMP-PVP can be potentially used as effective T_2-weighted MRI contrast agents.

EXPERIMENTAL

The details of the materials, instruments, and experimental procedures can be found in the electronic supplementary information (ESI).

All animal procedures were approved by the Institutional Animal Care and Use Committee (IACUC) of Tongji University (Ethics Approval Number: TJAA08124402).

RESULTS AND DISCUSSION

Synthesis and Characterization of MIONs@PTMP-PVP

Using the high-temperature co-precipitation method developed by Li *et al*.,[41] MIONs were synthesized by the co-precipitation of an aqueous iron precursor solution containing Fe^{3+} and Fe^{2+} (molar ratio 2:1) by ammonia in the presence of PTMP-PVP. The synthesis protocol is shown in Scheme 1(a).

As we know, rapid injection of precursors can lead to the supersaturation of reactants in the chemical mixture, which

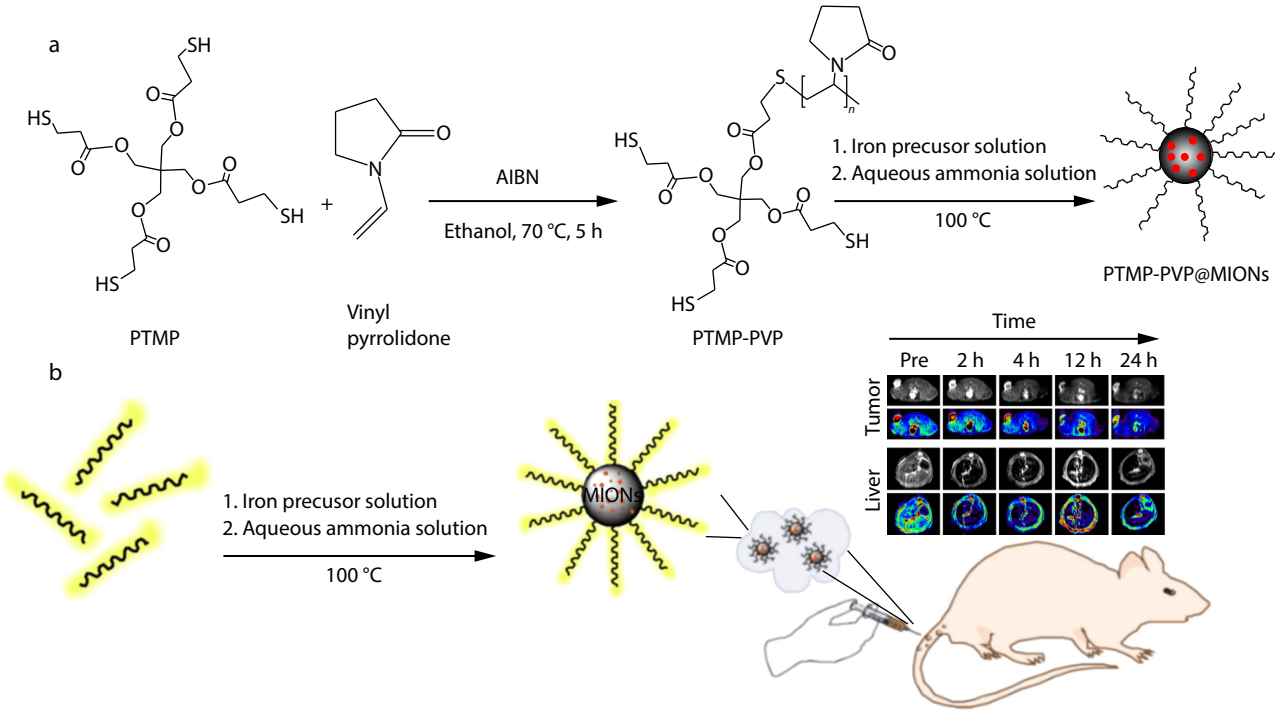

Scheme 1 (a) Graphical representation of the synthesis of polymer ligand PTMP-PVP and subsequent PTMP-PVP@MIONs preparation; (b) The synthesis protocol of MIONs@PTMP-PVP and its liver MR imaging application.

causes an initial burst of nucleation at once followed by the growth of nuclei, leading to the formation of monodisperse inorganic NPs. What's more, the presence of HCl in the precursors can avoid hydrolysis and condensation prior to the addition of precipitation agents. The size, shape and magnetic properties of the MIONs were controlled by using different concentration of polymer ligand during their preparation.

In order to determine the actual size of MIONs, TEM analysis was performed. As shown in Figs. 1(a) and 1(b), MIONs prepared with PTMP-PVP had a very small size of (11.7±1.5) nm. Fig. 1(c) shows the DLS of MIONs prepared with PTMP-PVP. The hydrodynamic size is approximately 44 nm. The actual size of the MIONs determined by TEM was smaller than that obtained by DLS, which is attributed to the presence of the extended layer of the hydrated polymer ligand around nanoparticles in aqueous media.[46]

The FTIR spectrum is shown in Fig. 1(d), where the band at 1662 cm^{-1} corresponds to the carbonyl groups (—CO—) of the pyrrolidone group of the polymer ligand, which shifted to 1627 cm^{-1} in the FTIR spectrum of MIONs@PTMP-PVP, indicating the interaction of the —CO— groups to the NPs surface. The band at 1294 cm^{-1} is due to the C—N stretching vibration of the pyrrolidone group of the polymer ligand. The characteristic absorption bands at 590 and 584 cm^{-1} in the FTIR spectrum of MIONs@PTMP-PVP belong to the stretching vibration mode of the Fe—O bonds in iron oxide NPs.[40] Overall, these FTIR spectra suggest the incorporation of PTMP-PVP into the MIONs.

To further verify the attachment of PTMP-PVP to MIONs and investigate the thermal stability of the MIONs@PTMP-PVP, thermogravimetric analysis (TGA) was performed using a TGA Q500 (Fig. 1e). MIONs@PTMP-PVP was reduced by approximately 90% at 460 °C, while bare MIONs showed no obvious change. It was concluded that the MIONs accounted for 10% of the weight of MIONs@PTMP-PVP.

The crystalline structure and phase of the iron oxide in MIONs@PTMP-PVP were determined by XRD analysis (Fig. 1f). It can be clearly seen that the peaks present at 2θ=32.9°, 35.7°, 40.5°, 47.0°, 52.9°, 58.5°, 68.5°, and 78.2° corresponding to the (220), (311), (222), (400), (422), (511), (440), and (533) reflections of magnetite, respectively, indicating the presence of crystalline spinel structured magnetite (Fe_3O_4) phase of iron oxide.

Salt stability tests were performed with aqueous dispersions of MIONs@PTMP-PVP and were found to be stable up to a high salt (NaCl) concentration (2.5 mol/L) (Fig. 2a). The hydrodynamic diameters in different concentrations of NaCl solution after 24 h and the relaxivity time (T_1 and T_2) in RPMI Medium 1640 (10% FBS) in different times did not change significantly (Figs. 2b and 2c).

Magnetic Properties Characterization and *In vitro* MRI

The magnetic curves of the MIONs@PTMP-PVP were obtained by cycling the magnetic field between –10 and +10 kOe. As shown in Fig. 3(a), MIONs@PTMP-PVP have a high saturation magnetization of 58 emu/g without any evident remanence or coercivity at 300 K, which is lower than the bare MIONs (70 emu/g).[47] It should be noted that, for MIONs@PTMP-PVP, the saturation magnetization has been corrected for the contribution from the magnetically dead polymer layer around the NPs, as determined by TGA (Fig. 1e).

To determine the relaxivity of MIONs@PTMP-PVP in water solution, longitudinal (T_1) and transverse proton relaxation times (T_2) were measured at various Fe^{3+} concentrations using a minispec mq 60 NMR analyzer (Bruker, Germany) operating at 1.41 T and 37 °C. Different concentrations of

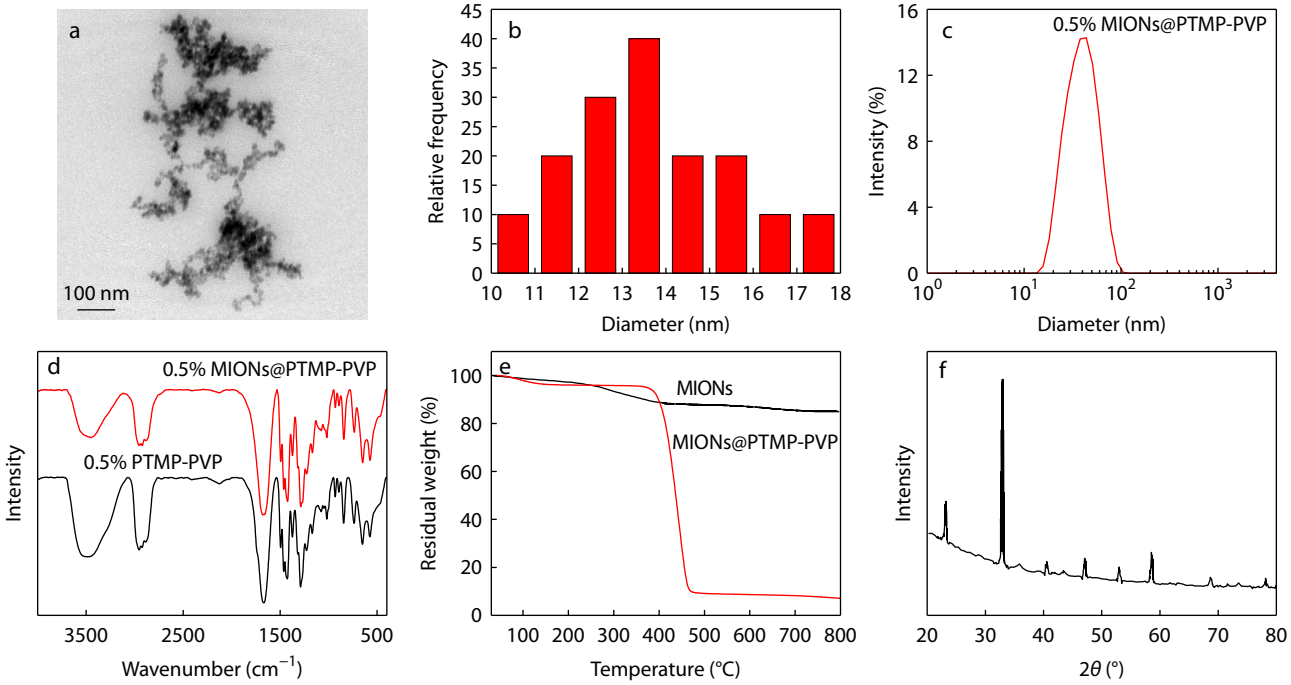

Fig. 1 (a) TEM image of MIONs@PTMP-PVP; (b) Particle size distribution histograms of MIONs@PTMP-PVP; (c) DLS data of MIONs@PTMP-PVP in water; (d) FTIR spectra of PTMP-PVP and MIONs@PTMP-PVP; (e) TGA curves of bare MIONs and MIONs@PTMP-PVP; (f) XRD pattern of MIONs@PTMP-PVP.

https://doi.org/10.1007/s10118-025-3522-4

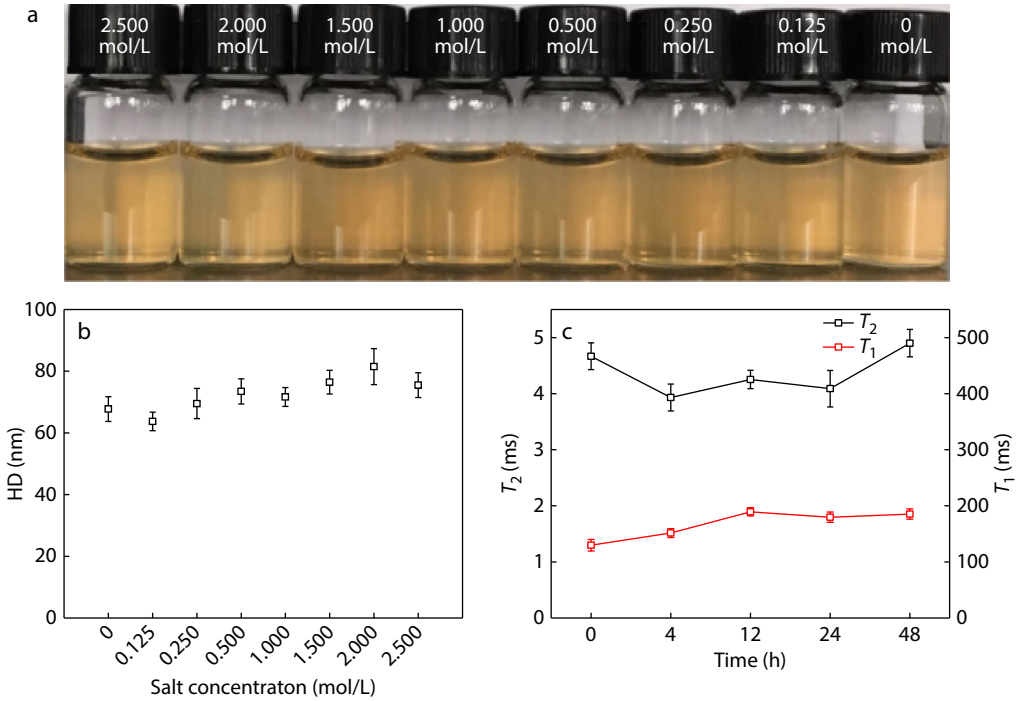

Fig. 2 (a) Images and (b) hydrodynamic diameters of MIONs@PTMP-PVP at different concentrations of NaCl solution after 24 h; (c) Relaxivity time (T_1 and T_2) of MIONs@PTMP-PVP in RPMI Medium 1640 (10% FBS) with different time.

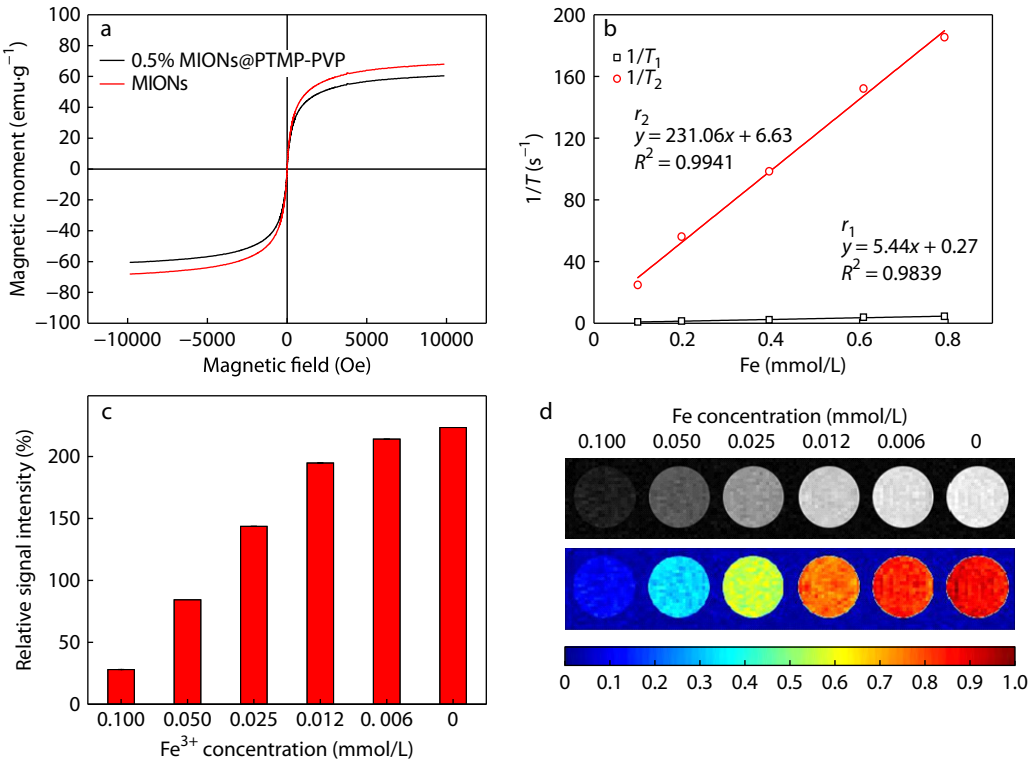

Fig. 3 (a) Magnetization curves of bare MIONs and MIONs@PTMP-PVP; (b) T_1 relaxation rates ($1/T_1$) and T_2 relaxation rates ($1/T_2$) of MIONs@PTMP-PVP; (c) Corresponding relative signal intensities under different Fe concentrations; (d) T_2-weighted images of MIONs@PTMP-PVP under different Fe concentrations.

MIONs@PTMP-PVP for relaxivity characterization were obtained by diluting with deionized water. As shown in Fig. 3(b), the r_2 relaxivity is 231.06 L·mmol^{-1}·s^{-1}, such a high r_2 relaxivity makes MIONs@PTMP-PVP capable of being a kind of T_2 contrast. Fig. 3(c) shows T_2-weighted images of MIONs@PTMP-PVP *in vitro* with decreasing Fe concentrations (from left to

https://doi.org/10.1007/s10118-025-3522-4

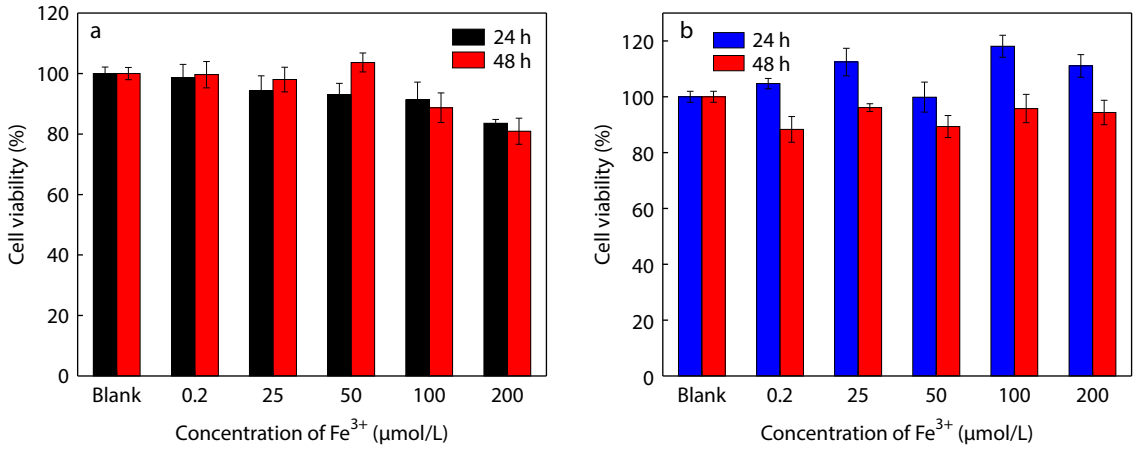

Fig. 4 Cytotoxicities of MIONs@PTMP-PVP under different Fe concentrations to DC 2.4 cells (a) and MCF-7 cells (b) determined by the CCK-8 cell proliferation assay.

right). Correspondingly, the signal brightness increases as the Fe concentration decreases. This trend is further demonstrated in Fig. 3(d).

It is therefore concluded that owing to its high relaxivity, MIONs@PTMP-PVP can be a potential candidate as an MRI contrast agent.

Cytotoxicity Study of MIONs@PTMP-PVP

The biocompatibility of the MIONs@PTMP-PVP was determined through an *in vitro* cytotoxicity analysis performed on DC 2.4 (dendritic cells). Fig. 4(a) shows the percent cell viability of DC 2.4, which was determined by the CCK-8 assay, after incubation of cells with different concentrations of MIONs for 24 and 48 h. Cell viability determined at zero concentration of MIONs was taken as 100%. MIONs@PTMP-PVP exhibited negligible toxicity for DC 2.4. As a result, cell viability was maintained at a high level (>80%), even when incubated with concentrated Fe (200 μmol/L). The cytotoxicity study of MCF-7 cells was similar, and cell viability was higher (Fig. 4b). These cytotoxicity data indicate the great potential of the MIONs@PTMP-PVP for *in vivo* imaging.

In vivo MRI Study and Biodistribution of MIONs@PTMP-PVP

To evaluate *in vivo* biodistribution, ICR female mice were injected with 2.5 mg Fe per kg body weight of MIONs@PTMP-PVP *via* the tail vein. At different time points post-injection, mice were anesthetized and sacrificed. The main organs were removed for inductively coupled plasma atomic emission spectroscopy (ICP-AES) analysis of Fe (Fig. 5). ICP analysis shows uptake and retention of MIONs@PTMP-PVP primarily in the liver. The concentration of Fe in the liver gradually decreased.

Iron oxide nanoparticles have been extensively developed for the diagnosis of liver diseases because they are highly taken up by the hepatic Kupffer cells. Thus, we focused on the liver as the target region to evaluate the *in vivo* MRI effects of MIONs@PTMP-PVP. Liver T_2-weighted MRI was obtained *in vivo* before and after the intravenous injections of MIONs@PTMP-PVP at the dosage of 2.5 mg Fe per kg body weight. As shown in Fig. 6, hypointensities induced by MIONs@PTMP-PVP can be readily observed in the liver at 10 min after injection. The contrast in the liver began to decrease 8 h after injection because of liver clearance. To quantify the contrast enhancement, we calculated the signal-to-noise ratio (SNR) by finely analyzing the regions of interest (ROIs) of the transverse images and defined the contrast enhancement as the decrease of the SNR (ΔSNR = (SNRpost-SNRpre)/SNRpre). Contrast enhancement indicated the accumulation of MIONs@PTMP-PVP in the liver, demonstrating that MIONs@PTMP-PVP can potentially be used as an effective T_2-weighted MRI contrast agent.

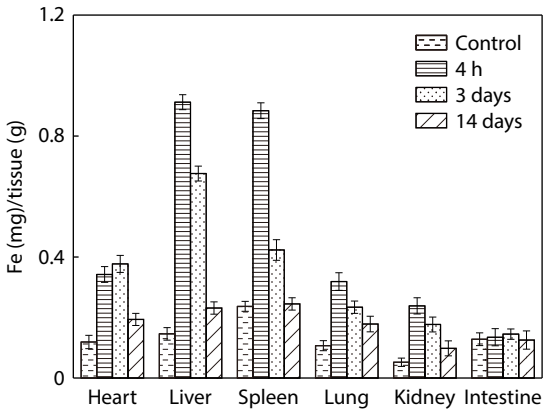

Fig. 5 Biodistributions in organs of mice with intravenous injection of MIONs@PTMP-PVP at the dosage of 2.5 mg Fe per kg body weight at different time points.

Histological Analysis

To further study the toxicity of MIONs@PTMP-PVP *in vivo*, histological assessment of tissues was conducted to determine tissue damage, inflammation, or lesions from toxic exposure. Tissues obtained from the harvested organs were analyzed to assess signs of potential toxicity. Histological analysis can be carried out by administration of MIONs@PTMP-PVP into mice in a subsequent 14 days period.

The liver, heart, spleen, hung, kidney, and intestines were chosen for the *in vivo* test because they retained most of the injected nanoparticles. All investigated organs of the experimental mice were normal, preserving the same structures as those of the control group, as shown in Fig. 7. Hepatocytes in the liver and spleen samples appeared normal, and there were no inflammatory infiltrates. The glomerulus structure

https://doi.org/10.1007/s10118-025-3522-4

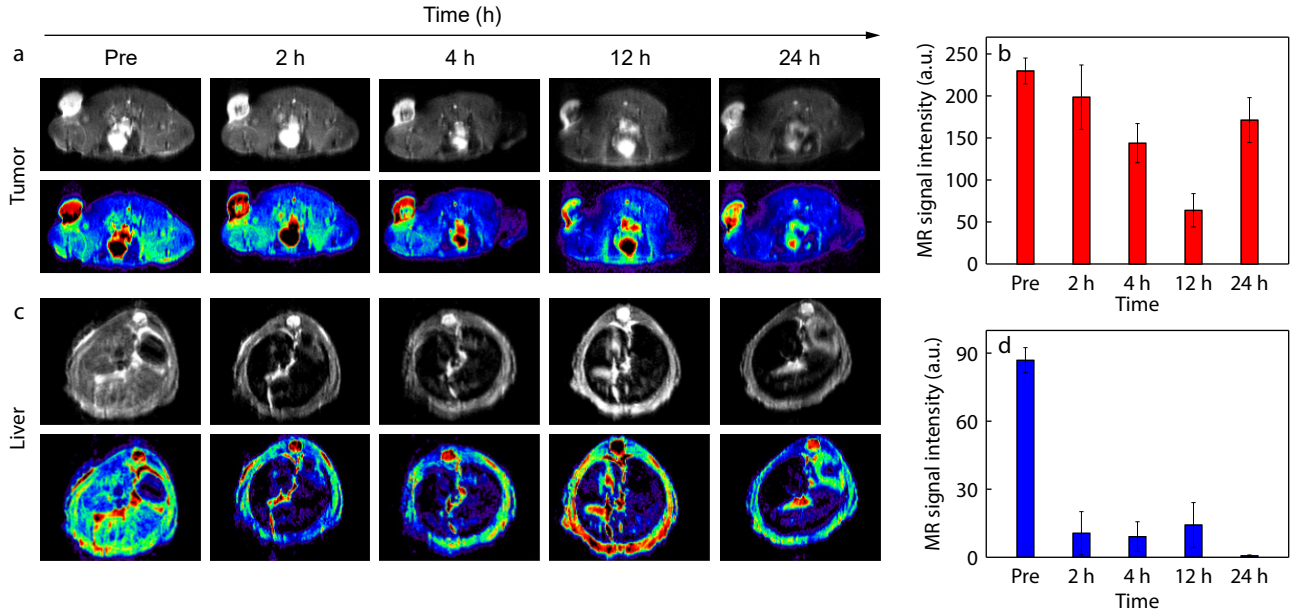

Fig. 6 *In vivo* MR imaging guidance in tumor-bearing mice. (a) Time-dependent *in vivo* MR of tumor before and after intravenous injection of MIONs@PTMP-PVP at the dosage of 2.5 mg Fe per kg body weight; (b) The corresponding-weighted MR signal of tumor; (c) Time-dependent *in vivo* MR of Liver before and after intravenous injection of MIONs@PTMP-PVP at the dosage of 2.5 mg Fe per kg body weight; (d) The corresponding-weighted MR signal of Liver.

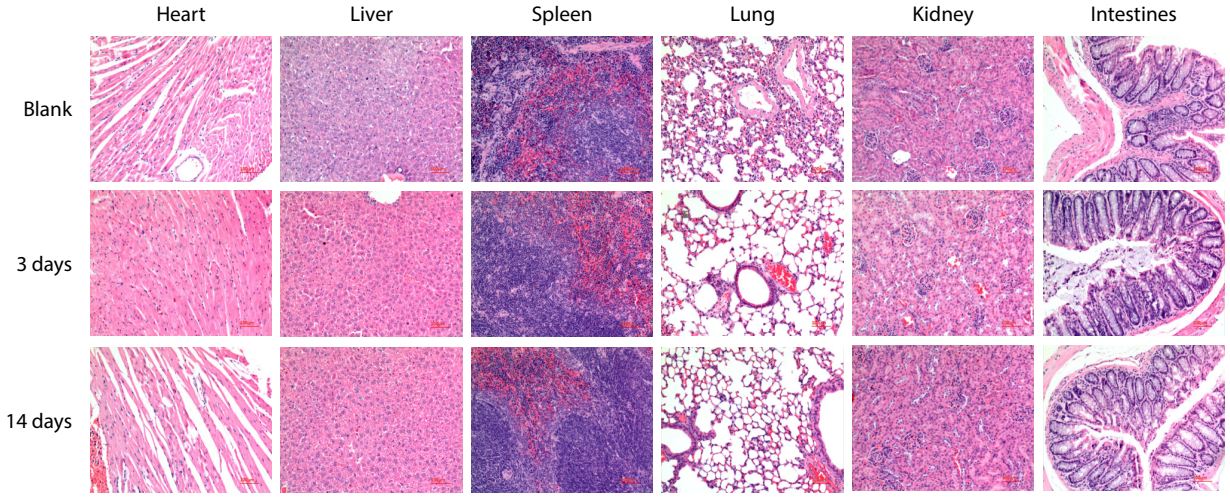

Fig. 7 H&E staining tissue sections from injected mice after 3 and14 days compared with those in healthy mice.

could be easily distinguished in the kidney samples. No necrosis was found in any group. The observed biocompatibility is attributable to green chemical synthesis.

CONCLUSIONS

In summary, we have successfully prepared novel magnetic iron oxide nanoparticles coated with PTMP-PVP. The obtained MIONs@PTMP-PVP exhibited excellent water solubility and high stability in NaCl solutions across a concentration range of 0–2.5 mol/L. *In vivo* MRI results demonstrate the promising potential of MIONs@PTMP-PVP as a liver-specific magnetic resonance imaging agent. Biodistribution analysis further indicated that these nanoparticles were primarily taken up and retained in the liver. Both the *in vitro* CCK-8 assay and *in vivo* histological analysis confirmed the very low toxicity. These MIONs also showed high relaxivity and improved MRI contrast performance. Based on the comprehensive experimental results, MIONs@PTMP-PVP demonstrated great potential for liver-specific magnetic resonance imaging.

Conflict of Interests

The authors declare no interest conflict.

Electronic Supplementary Information

Electronic supplementary information (ESI) is available free of charge in the online version of this article at http://doi.org/10.1007/s10118-025-3522-4.

Data Availability Statement

The data that support the findings of this study are available from the corresponding author upon reasonable request.

ACKNOWLEDGMENTS

This work was financially supported by the International Cooperation Program from the Ministry of Science and Technology of Hubei Province (No. 2023EHA069), Shenzhen Science and Technology Program (No. JCYJ20230807143702005), and National Foreign Experts Program (No. G2022027015L).

REFERENCES

1 Gong, F.; Zhang, Z.; Chen, X.; Zhang, L.; Yu, X.; Yang, Q.; Shuai, X.; Liang, B.; Cheng, D. A dual ligand targeted nanoprobe with high MRI sensitivity for diagnosis of breast cancer. *Chinese J. Polym. Sci.* **2014**, *32*, 321–332.
2 Wang, H.; Dai, T.; Lu, B.; Li, S.; Lu, Q.; Mukwaya, V.; Dou, H. Hybrid dextran-gadolinium nano-suitcases as high-relaxivity MRI contrast agents. *Chinese J. Polym. Sci.* **2018**, *36*, 391–398.
3 Zhang, T.; Cheng, Q.; Cheng, H.; Wang, Q.; Wang, B.; Zhang, B.;

Graphical Abstract

Water-soluble Polymer Ligand Mediated Synthesis of Superparamagnetic Iron Oxide Nanoparticles for Magnetic Resonance Imaging

Ping-Ting Gong, Jiao-Jiao Guo, Chang Gao, Wei-Tao Yang, Chun-Sheng Xiao, Yi Xu, Yue Yao, Irshad Hussain, Wen Fan, and Wei Yan

Hubei University, China; Shenzhen Huazhong University of Science and Technology Research Institute, China; Tongji University, China; Changchun Institute of Applied Chemistry, Chinese Academy of Sciences, China; The University of Hong Kong, China; Lahore University of Management Sciences (LUMS), Pakistan

Using high-temperature co-precipitation method, super paramagnetic iron oxide nanoparticles (MIONs) were synthesized in the presence of polymer ligand pentaerythritol tetrakis 3-mercaptopropionate-poly(*N*-vinyl-2-pyrrolidone) (PTMP-PVP). These nanoparticles were demonstrated by *in vivo* magnetic resonance imaging (MRI) studies to be promising T_2-weighted contrast agent.

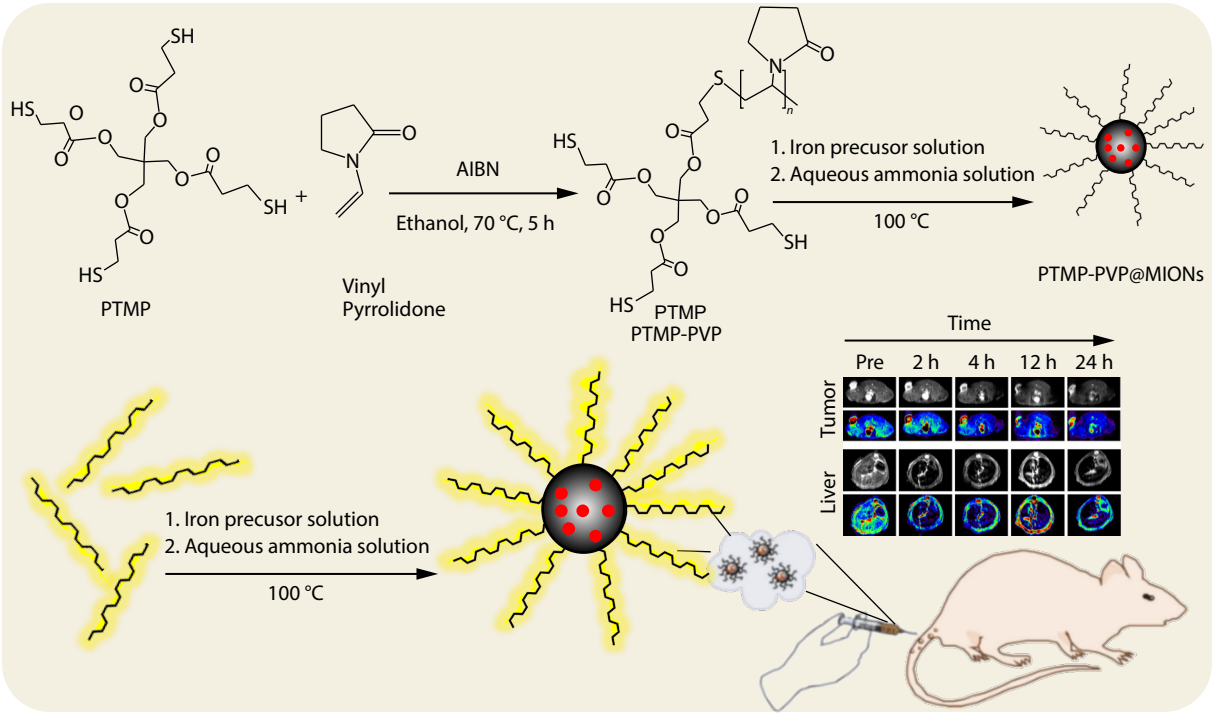

Chinese J. Polym. Sci. 2026, 44, 407–415 *https://doi.org/10.1007/s10118-025-3522-4*

Sun, H.; Deng, C.; Tang, Z. Manipulation of magnetic edge states in carbon quantum dots for magnetic resonance imaging and NIR-II photo-thermoelectric therapy. *Nat. Commun.* **2025**, *16*, 5867.
4 Lu, C.; Liao, S.; Chen, B.; Xu, L.; Wu, N.; Lu, D.; Kang, H.; Zhang, X.; Song, G. Responsive probes for in vivo magnetic resonance imaging of nitric oxide. *Nat. Mater.* **2025**, *24*, 133–142.
5 Wallstein, N.; Capucciati, A.; Pöppl, A.; Schnohr, C. S.; Sturini, M.; Pampel, A.; Jäger, C.; Zecca, L.; Zucca, F. A.; Monzani, E.; Casella, L.; Möller, H. E. Modeling midbrain and brainstem neuromelanins to characterize metal binding and associated MRI contrast in parkinson's and alzheimer's diseases. *Angew. Chem. Int. Ed.* **2025**, *64*, e202509102.
6 Rezaei, B.; Tay, Z. W.; Mostufa, S.; Manzari, O. N.; Azizi, E.; Ciannella, S.; Moni, H.E.J.; Li, C.; Zeng, M.; Gómez-Pastora, J.; Wu, K. Magnetic nanoparticles for magnetic particle imaging (MPI): design and applications. *Nanoscale* **2024**, *16*, 11802–11824.
7 Lazovic, J.; Goering, E.; Wild, A.M.; Schützendübe, P.; Shiva, A.; Löffler, J.; Winter, G.; Sitti, M. Nanodiamond-enhanced magnetic resonance imaging. *Adv. Mater.* **2024**, *36*, 2310109.
8 Wang, G.; Angelovski, G. Highly potent MRI contrast agent displaying outstanding sensitivity to zinc ions. *Angew. Chem. Int. Ed.* **2021**, *60*, 5734–5738.
9 Chen, J.; Shen, Y.; Yu, Q.; Gan, Z. Paclitaxel prodrug nanomedicine for potential CT-imaging guided breast cancer therapy. *Chinese J. Polym. Sci.* **2023**, *41*, 1747–1759.
10 Ma, Z.; Li, D.; Jia, X.; Wang, R.; Zhu, M. Recent advances in bio-Inspired versatile polydopamine platforms for "smart" cancer photothermal therapy. *Chinese J. Polym. Sci.* **2023**, *41*, 699–712.
11 Ji, S.; Lan, H.; Zhou, S.; Zhang, X.; Chen, W.; Jiang, X. Ir(III)-based ratiometric hypoxic probe for cell imaging. *Chinese J. Polym. Sci.* **2023**, *41*, 794–801.
12 Liu, C.; Li, L.; Guo, Z.; Lin, L.; Li, Y.; Tian, H. PLG-g-mPEG mediated multifunctional nanoparticles for photoacoustic imaging guided combined chemo/photothermal antitumor therapy. *Chinese J. Polym. Sci.* **2023**, *41*, 538–546.
13 Chen, X. S. Biomedical polymers--escort for human health. *Chinese J. Polym. Sci.* **2022**, *40*, 1004–1005.
14 Wu, W.; Yan, X.; Chen, S.; Du, Y.; Hu, J.; Song, Y.; Zha, Z.; Xu, Y.; Cao, B.; Xuan, S.; Liu, X.; Chen, B.; Dong, L.; Lu, Y.; Yu, S. Minimally invasive delivery of percutaneous ablation agent via magnetic colloidal hydrogel injection for treatment of hepatocellular carcinoma. *Adv. Mater.* **2024**, *36*, 2309770.
15 Zacharias, N. M.; Ornelas, A.; Lee, J.; Hu, J.; Davis, J. S.; Uddin, N.; Pudakalakatti, S.; Menter, D. G.; Karam, J. A.; Wood, C. G.; Hawk, E. T.; Kopetz, S.; Vilar, E.; Bhattacharya, P. K.; Millward, S. W. Real-time interrogation of aspirin reactivity, biochemistry, and biodistribution by hyperpolarized magnetic resonance spectroscopy. *Angew. Chem. Int. Ed.* **2019**, *58*, 4179–4183.
16 Maier, A.; Qi, J.; Shukla, K.; Dugulan, A. I.; Hagedoorn, P.; Oossanen, R.; Rhoon, G.; Denkova, A. G.; Djanashvili, K. Enhancing magnetic hyperthermia efficiency in Pd/Fe-oxide hybrid nanoparticles through Mn-doping. *ACS Appl. Nano Mater.* **2024**, *7*, 27465–27475.
17 Stepanov, A.; Fedorenko, S.; Mendes, R.; Rümmeli, M.; Giebeler, L.; Weise, B.; Gemming, T.; Dutz, S.; Zahn, D.; Ismaev, I.; Amirov, R.; Kholin, K.; Voloshina, A.; Sapunova, A.; Solovieva, S.; Mustafina, A. T_2 and T_1 relaxivities and magnetic hyperthermia of iron-oxide nanoparticles combined with paramagnetic Gd complexes. *J. Chem. Sci.* **2021**, *133*, 43.
18 Zhang, L.; Tong, S.; Zhang, Q.; Bao, G. Lipid-encapsulated Fe_3O_4 nanoparticles for multimodal magnetic resonance/fluorescence imaging. *ACS Appl. Nano Mater.* **2020**, *3*, 6785–6797.
19 Clough, T. J.; Jiang, L.; Wong, K.; Long, N. J. Ligand design strategies to increase stability of gadolinium-based magnetic resonance imaging contrast agents. *Nat. Commun.* **2019**, *10*, 1420.
20 Chen, X.; Teng, S.; Li, J.; Qiao, X.; Zhao, W.; Xue, Z.; Shi, X.; Wang, Y.; Yang, W.; Wang, T. Gadolinium (III)-chelated deformable mesoporous organosilica nanoparticles as magnetic resonance imaging contrast agent. *Adv. Mater.* **2023**, *35*, 2211578.
21 Qin, R.; Li, S.; Qiu, Y.; Feng, Y.; Liu, Y.; Ding, D.; Xu, L.; Ma, X.; Sun, W.; Chen, H. Carbonized paramagnetic complexes of Mn (II) as contrast agents for precise magnetic resonance imaging of sub-millimeter-sized orthotopic tumors. *Nat. Commun.* **2022**, *13*, 1938.
22 Yu, K. C.; Hu, H. B.; Liu, M. L.; Yuan, H. Z.; Ye, C. H.; Zhuo, R. X. NMR relaxivity and imaging of neutral macromolecular polyester gadolinium (III) complexes. *Chinese J. Polym. Sci.* **1999**, *17*, 471–475.
23 Du, H.; Yu, J.; Guo, D.; Yang, W.; Wang, J.; Zhang, B. Improving the MR imaging sensitivity of upconversion nanoparticles by an internal and external incorporation of the Gd^{3+} strategy for in vivo tumor-targeted imaging. *Langmuir* **2016**, *32*, 1155–1165.
24 Ognjanović, M.; Kolev, H.; Mladenova, R.; Vojtova, J.; Strbak, O.; Fabián, M.; Girman, V.; Dojčinović, B.; Vranješ-Durić, S.; Antić, B. Ultra-low gadolinium doping in multi-core iron oxide enables efficient dual-mode MRI and magnetic hyperthermia: a structure-function study. *Nanoscale* **2025**, *17*, 23727–23739.
25 Wang, J.; Liang, K.; Li, J.; Zhang, Y.; Xue, X.; Chen, T.; Hao, Y.; Wu, J.; Ge, J. H_2O_2-Responsive injectable polymer dots hydrogel for long-term photodynamic therapy of tumors. *Chinese J. Polym. Sci.* **2024**, *42*, 1690–1698.
26 Feng, W.; Wu, Y.; Liu, X.; Wang, Z. Shear-thinning catechol-modified chitosan hydrogel loaded with silver nanoparticles for endoscopic submucosal dissection. *Chinese J. Polym. Sci.* **2024**, *42*, 1147–1155.
27 Singh, P.; Pandit, S.; Balusamy, S. R.; Madhusudanan, M.; Singh, H.; Haseef, H. M. A.; Mijakovic, I. Advanced nanomaterials for cancer therapy: gold, silver, and iron oxide nanoparticles in oncological applications. *Adv. Healthc. Mater.* **2025**, *14*, 2403059.
28 Zhang, H.; Mao, Y.; Nie, Z.; Li, Q.; Wang, M.; Cai, C.; Hao, W.; Shen, X.; Gu, N.; Shen, W.; Song, H. Iron oxide nanoparticles engineered macrophage-derived exosomes for targeted pathological angiogenesis therapy. *ACS Nano* **2024**, *18*, 7644–7655.
29 Ye, D.; Li, M.; Xie, Y.; Chen, B.; Han, Y.; Liu, S.; Wei, Q.; Gu, N. Optical imaging and high-accuracy quantification of intracellular iron contents. *Small* **2021**, *17*, 2005474.
30 Abdullah, M.; Nelson, R. J.; Kittilstved, K. R. Tunable redox activity at Fe^{3+} centers in colloidal $ATiO_3$ (A = Sr and Ba) nanocrystals. *Chem. Mat.* **2021**, *33*, 4196–4203.
31 Zhang, H.; Guo, Y.; Jiao, J.; Qiu, Y.; Miao, Y.; He, Y.; Li, Z.; Xia, C.; Li, L.; Cai, J.; Xu, K.; Liu, X.; Zhang, C.; Bay, B.; Song, S.; Yang, Y.; Peng, M.; Wang, Y.; Fan, H. A hepatocyte-targeting nanoparticle for enhanced hepatobiliary magnetic resonance imaging. *Nat. Biomed. Eng.* **2023**, *7*, 221–235.
32 Lu, Y.; Xu, Y.; Zhang, G.; Ling, D.; Wang, M.; Zhou, Y.; Wu, Y.; Wu, T.; Hackett, M. J.; Kim, B. H.; Chang, H.; Kim, J.; Hu, X.; Dong, L.; Lee, N.; Li, F.; He, J.; Zhang, L.; Wen, H.; Yang, B.; Choi, S. H.; Hyeon, T.; Zou, D. Iron oxide nanoclusters for T_1 magnetic resonance imaging of non-human primates. *Nat. Biomed. Eng.* **2017**, *1*, 637–643.
33 Ghasemzadeh, H.; Dargahi, M.; Eyvazi, G.; Farahani, B. V. Nanomagnetic organogel based on dodecyl methacrylate for absorption and removal of organic solvents. *Chinese J. Polym. Sci.* **2019**, *37*, 444–450.
34 Ilosvai, Á. M.; Heydari, F.; Forgách, L.; Kovács, N.; Szigeti, K.; Máthé, D.; Kristály, F.; Daróczi, L.; Viskolcz, B.; Nagy, M.; Németh, M.; Ollár, T.; Vanyorek, L. Development of manganese ferrite coated with prussian blue as an efficient contrast agent for applications in

magnetic resonance imaging. *Sci. Rep.* **2025**, *15*, 14150.
35 Laha, S. S.; Thorat, N. D.; Singh, G.; Sathish, C. I.; Yi, J.; Dixit, A.; Vinu, A. Rare-earth doped iron oxide nanostructures for cancer theranostics: magnetic hyperthermia and magnetic resonance imaging. *Small* **2022**, *18*, 2104855.
36 Hu, C.; Xia, T.; Gong, Y.; Wang, X.; Liu, R.; Zhang, Q.; Yi, C.; Xu, Z.; Guo, D. Emulsifier-free emulsion polymerized poly (MMA-HEMA-Eu(AA)$_3$Phen)/Fe_3O_4 magnetic fluorescent bifunctional nanospheres for magnetic resonance and optical imaging. *Chinese J. Polym. Sci.* **2016**, *34*, 135–146.
37 Zhang, Y.; Wang, X.; Guo, M.; Yan, H.; Wang, C.; Liu, K. Cisplatin-loaded polymer/magnetite composite nanoparticles as multifunctional therapeutic nanomedicine. *Chinese J. Polym. Sci.* **2014**, *32*, 1329–1337.
38 Schumacher, M. L.; Britos, T. N.; Fonseca, F. L. A.; Ferreira, F. F.; Feder, D.; Fratini, P.; Petri, G.; Haddad, P. S. Superparamagnetic nanoparticles as potential drug delivery systems for the treatment of duchenne muscular dystrophy. *Nanoscale* **2025**, *17*, 3752–3767.
39 Majeed, M. I.; Lu, Q.; Yan, W.; Li, Z.; Hussain, I.; Tahir, M. N.; Tremel, W.; Tan, B. Highly water-soluble magnetic iron oxide (Fe_3O_4) nanoparticles for drug delivery: enhanced in vitro therapeutic efficacy of doxorubicin and MION conjugates. *J. Mat. Chem. B* **2013**, *1*, 2874–2884.
40 Majeed, M. I.; Guo, J.; Yan, W.; Tan, B. Preparation of magnetic iron oxide nanoparticles (MIONs) with improved saturation magnetization using multifunctional polymer ligand. *Polymers* **2016**, *8*, 392.
41 Li, Z.; Yi, P.; Sun, Q.; Lei, H.; Zhao, H.; Zhu, Z.; Smith, S. C.; Lan, M.; Lu, G. Ultrasmall water-soluble and biocompatible magnetic iron oxide nanoparticles as positive and negative dual contrast agents. *Adv. Funct. Mater.* **2012**, *22*, 2387–2393.
42 Laroui, A.; Kelland, M. A.; Wang, D.; Xu, S.; Xu, Y.; Lu, P.; Dong, J. Kinetic Inhibition of clathrate hydrate by copolymers based on N-vinylcaprolactam and N-acryloylpyrrolidine: optimization effect of interfacial nonfreezable water of polymers. *Langmuir* **2022**, *38*, 1522–1532.
43 Xu, Q.; Yuan, Z.; Wang, C.; Liang, H.; Shi, Y.; Wu, H.; Xu, H.; Zheng, J.; Wu, J. Tough semi-interpenetrating polyvinylpyrrolidone/polyacrylamide hydrogels enabled by bioinspired hydrogen-bonding induced phase separation. *Chinese J. Polym. Sci.* **2024**, *42*, 591–603.
44 Xu, G.; Hu, X.; Liao, X.; Chen, Y. Bending-stability interfacial layer as dual electron transport layer for flexible organic photovoltaics. *Chinese J. Polym. Sci.* **2021**, *39*, 1441–1447.
45 Meng, X.; Yu, G.; Ma, J. Preparation and properties of poly(aryl ether sulfone ketone) ultrafiltration membrane containing fluorene group for high temperature condensed water treatment. *Chinese J. Polym. Sci.* **2018**, *36*, 970–978.
46 Xie, J.; Xu, C.; Kohler, N.; Hou, Y.; Sun, S. Controlled PEGylation of monodisperse Fe3O4 nanoparticles for reduced non-specific uptake by macrophage cells. *Adv. Mater.* **2007**, *19*, 3163–3166.
47 Ge, R.; Li, X.; Lin, M.; Wang, D.; Li, S.; Liu, S.; Tang, Q.; Liu, Y.; Jiang, J.; Liu, L.; Sun, H.; Zhang, H.; Yang, B. Fe_3O_4@polydopamine composite theranostic superparticles employing preassembled Fe3O4 nanoparticles as the core. *ACS Appl. Mater. Interfaces* **2016**, *8*, 22942–22952.

https://doi.org/10.1007/s10118-025-3522-4